Muon-spin-rotation study of Ce_7Ni_3: muon-related and intrinsic properties of the paramagnetic phase

2001 J. Phys.: Condens. Matter 13 4277

(http://iopscience.iop.org/0953-8984/13/19/308)

INSTITUTE OF PHYSICS PUBLISHING JOURNAL OF PHYSICS: CONDENSED MATTER

J. Phys.: Condens. Matter **13** (2001) 4277–4290 www.iop.org/Journals/cm PII: S0953-8984(01)19917-0

Muon-spin-rotation study of Ce_7Ni_3: muon-related and intrinsic properties of the paramagnetic phase

A Schenck[1], D Andreica[1], F N Gygax[1], K Umeo[2], T Takabatake[2], E Schreier[3], A Kratzer[3] and G M Kalvius[3]

[1] Institute for Particle Physics of ETHZ, CH-5232 Villigen PSI, Switzerland
[2] Department of Quantum Matter, Graduate School of Advanced Sciences of Matter, Hiroshima University, Higashi-Hiroshima 739-8526, Japan
[3] Physics Department, TU München, D-85747 Garching, Germany

Received 8 December 2000, in final form 16 March 2001

Abstract

We report on transverse-field (0.6 T) muon-spin-rotation (μSR) measurements between 3 K and 300 K on single crystals of the hexagonal heavy-fermion compound Ce_7Ni_3 with the primary goal of determining the μ^+ lattice site(s). The μSR spectrum consists in each case of two components which are distinguished by their anisotropic, axially symmetric Knight shifts and which can be associated with two types of tetrahedrally coordinated b site (in Wyckoff notation). The relative occupation of the two sites varies with temperature and, surprisingly, depends also on the orientation of the crystals with respect to the applied field $\boldsymbol{B}_{ext}$. We find that below 80 K the muon Knight shift follows a perfect Curie–Weiss behaviour down to 3 K, exhibiting Curie temperatures of approximately ± 1 K in striking contrast to the behaviour of the bulk susceptibility. Above 100 K the Knight shift scales with the bulk susceptibility. In the transitional range 60 K–100 K muon diffusion sets in, probably proceeding by jumps via the two types of b site. Below 50 K an increasing part of the μSR signal appears to be wiped out ($\sim$30% at 3 K), signalling the presence of an internal static field spread above 1 kG, perhaps related to a persisting magnetic order above $T_N = 1.9$ K in part of the sample volume.

1. Introduction

The discovery of non-Fermi-liquid behaviour near a quantum critical point in some of the so-called heavy-fermion systems [1] has attracted considerable attention in recent years. Among these systems, stoichiometric Ce_7Ni_3 is prominent since the quantum critical point can be approached by applying hydrostatic pressure [2], while usually this involves chemical substitution which introduces a certain degree of randomness with unwanted side effects. Ce_7Ni_3 crystallizes in the hexagonal Th_7Fe_3-type structure (space group $P6_3mc$) in which Ce is found at three crystallographically inequivalent lattice sites [3] labelled as Ce_1, Ce_2, Ce_3 (see figure 1). Ce_7Ni_3 is characterized as a heavy-fermion system ($\gamma = 9$ J mol^{-1} K^{-2} [4])

0953-8984/01/194277+14$30.00

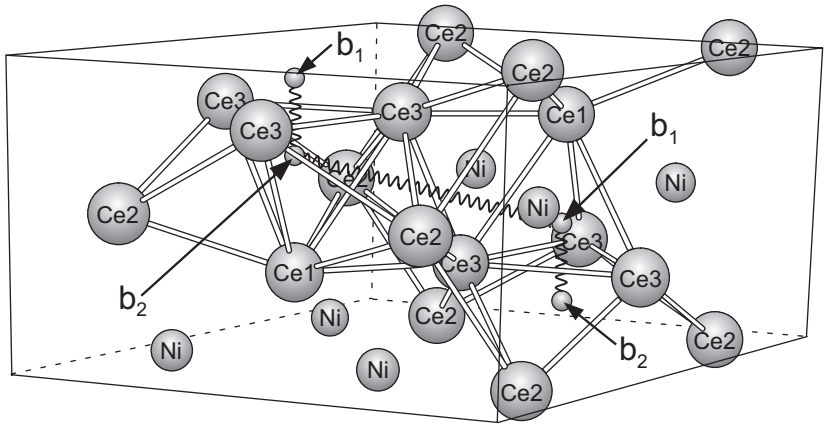

Figure 1. Crystal structure of hcp Ce_7Ni_3 (space group Pb_3mc). The Ce ions occupy three different crystallographic sites: Ce_1 at a b site (two per unit cell), Ce_2 at a c site (six per unit cell) and Ce_3 at another c site (six per unit cell). Also indicated are the two b sites occupied by the muons and the jump paths between two nearest-neighbour b_1 and b_2 sites and between b_1 and b_2 sites via the c site at the centre of the figure.

and orders antiferromagnetically below $T_N = 1.9$ K at ambient pressure. The incommensurate magnetic structure has been studied in detail by means of neutron scattering [5]. The magnetic susceptibility follows a Curie–Weiss behaviour above 100 K with paramagnetic Curie temperatures of -67 K and -24 K for the applied field $\boldsymbol{B}_{ext}$ perpendicular and parallel to the c-axis, respectively [2]. The effective magnetic moments per Ce atom are 2.61 μ_B and 2.52 μ_B, respectively, which are close to the free-Ce^{3+} Hund's-rule value of 2.54 μ_B. This observation indicated that at all three inequivalent sites, Ce is in the same trivalent state [2, 6]. Therefore there are no indications that the Ni ions contribute to the magnetic properties of Ce_7Ni_3.

μSR spectroscopy has been applied to this system with the aim of studying the magnetically ordered state on an atomic scale, thereby complementing neutron scattering measurements, and the spin dynamics above T_N [7]. The analysis of such data requires knowledge of the μ^+ site or sites. The primary aim of the present study was to identify the μ^+ site(s) from a measurement of the dipolar contribution to the μ^+ Knight shift. The dipolar coupling tensor depends only on the crystal structure and the μ^+ position and can be calculated from lattice sums [8]. Occupation of magnetically or crystallographically inequivalent sites may lead to a splitting of the transverse-field (TF) μSR signal, i.e. μ^+ may precess with slightly different frequencies. A second aim was to determine the local magnetic response and compare it with the bulk magnetic susceptibility. Such information may allow us to assess μ^+-induced modifications, and/or, in the case where the magnetic ions are associated with inequivalent sites, to find out whether their magnetic responses are different [9]. Finally, in view of the fact that implanted positive muons can be regarded as light protons, it is always of interest to study their static and dynamic behaviour (change of site occupation, diffusion, trapping) with regard to the physics of hydrogen in metals in the infinitely dilute limit.

This article is organized as follows: in the next section some experimental details are presented, section 3 contains the results and their analysis, in section 4 the determination of the μ^+ sites is detailed, section 5 deals with a comparison of the bulk susceptibility and the local susceptibility, section 6 addresses changes in site occupation and μ^+ dynamics and a summary and conclusions are presented in section 7.

2. Experimental details

Two single crystals of Ce_7Ni_3 of cylindrical shape were investigated. The first (second) crystal had a diameter of 3 mm (6.8 mm) and a length of 5.8 mm (5.7 mm). In both samples (No 1, No 2) the cylinder axes coincided with the crystallographic a-axis. Both crystals were cut from a larger parent crystal grown by the Czochralski method, using high-purity Ce (99.9%) and Ni (99.99%) metals produced by the Ames Laboratory and Johnson-Matthey Limited, respectively [10]. No impurity phase was observed by electron-probe microanalysis and metallographic examination. The low-temperature resistivity in Ce_7Ni_3 is dominated by spin fluctuations and one cannot characterize the quality of the crystal [11].

The μSR measurements in the transverse-field geometry were performed with the general-purpose spectrometer (GPS) on the πM3 beamline of the accelerator complex of the Paul Scherrer Institute (PSI) in Villigen, Switzerland. The applied field B_{ext} amounted generally to 0.6 T corresponding to a Larmor frequency of 81.3 MHz. The samples were mounted in a He-flow cryostat which allowed one to set temperatures between 3 K and 300 K. The first sample was mounted with the cylinder axis perpendicular to $\boldsymbol{B}_{ext}$. By rotating the sample around the cylinder axis, $\boldsymbol{B}_{ext}$ could be oriented parallel to the b^*-axis or c-axis; the second sample was mounted such that $\boldsymbol{B}_{ext}$ was parallel to the a-axis. The axes a, b^*, c form a cartesian coordinate system; b^* denotes the reciprocal b^*-axis. A special veto counter arrangement and an almost massless sample holder (a tube made out of Mylar foil) allowed suppression of the contribution to the μSR signal from muons not stopping in the sample to less than 5%.

The positrons from the muon decay were detected in three telescopes in up, down and right positions with respect to the μ^+ beam line, all positioned in a plane perpendicular to the applied field $\boldsymbol{B}_{ext}$. The initial μ^+ polarization was turned by a spin rotator from parallel to the beam direction towards the up–down direction by $\sim 50^\circ$. Hence the time evolution of the μ^+ polarization projected onto the up–down–right plane could be recorded.

The following measurements were made:

(i) An angular scan at 20 K, by rotating sample No 1 around the a-axis with $\boldsymbol{B}_{ext}$ lying in the (b^*, c) plane. The muons were entering the sample perpendicularly to the cylinder axis.
(ii) Temperature scans between 3 K and 300 K with the same sample, but with $\boldsymbol{B}_{ext}$ oriented parallel to either the c-axis or the b^*-axis, respectively.
(iii) A temperature scan with sample No 2 but with $\boldsymbol{B}_{ext}$ oriented parallel to the a-axis. In this case the muons entered the sample through a flat face of the cylinder.

3. Results

The TF measurements revealed generally three components in the μSR signal as can be seen from its Fourier transform displayed in figure 2. The small signal in the centre stems from the residual background signal; the two other peaks originate from the sample. Consequently the time evolution of the μ^+ polarization was fitted by the function

$$P(t) = \sum_{i=1}^{3} A_i \exp(-\lambda_i t) \cos(2\pi \nu_i + \varphi) \tag{1}$$

where the ν_i are the precession frequencies, A_i the amplitudes of the components, φ a phase which depends on the positron detector position. Best results were achieved by letting each component relax exponentially with a rate λ_i. A Gaussian damping proved to be less adequate. The fits were actually performed jointly to all three spectra collected with the up, down and right positron detectors. The background asymmetry A_3 amounted to about 1–2% and the background frequency ν_3 to 81.305 MHz.

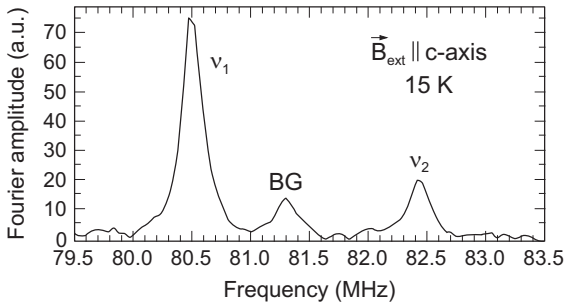

Figure 2. The Fourier transform (real amplitude) of a μSR spectrum taken at 15 K. BG denotes a background signal from μ^+ not stopping in the sample.

Figure 3(a) shows the angular dependences of ν_1 and ν_2 at 20 K, when rotating the applied field in the (b^*, c) plane. Both frequencies follow a $\cos^2\theta$ dependence. The angular dependence of λ_1 and λ_2 is displayed in figure 3(b). Interestingly λ_1 shows an isotropic behaviour, while λ_2 also follows a $\cos^2\theta$ dependence.

The temperature scans reveal that the amplitudes A_1 and A_2, which are measures of the fractions of μ^+ contributing to these signals (henceforth labelled as I and II), are strongly temperature dependent. The fit results are displayed in figure 4. Several striking observations can be made. Below roughly 50 K the sum of A_1 and A_2 starts to drop with decreasing temperature. The temperature dependence of the missing asymmetry is shown in the inset of

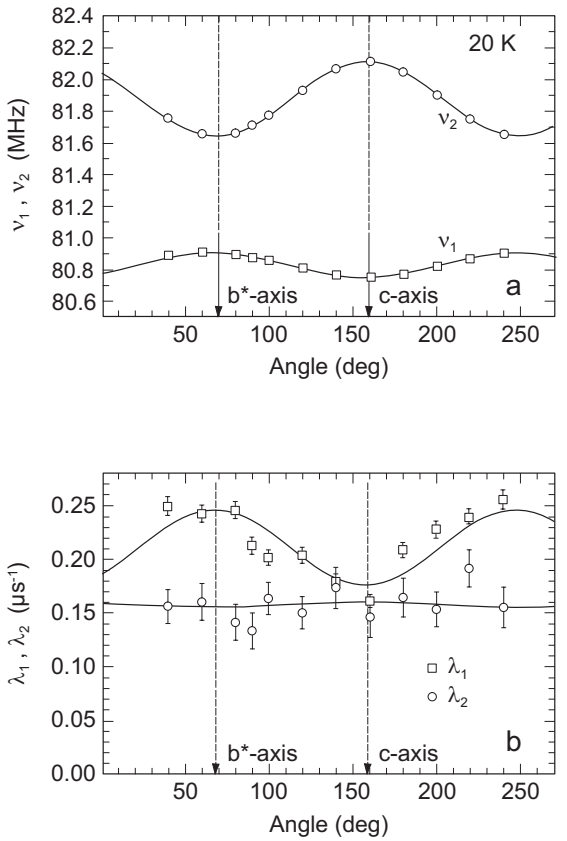

Figure 3. Orientation dependences of (a) the precession frequencies ν_1 and ν_2 and (b) the relaxation rates λ_1, λ_2 at 20 K when turning the applied field $\boldsymbol{B}_{ext}$ in the (b^*, c) plane. Indicated are the laboratory angles at which $\boldsymbol{B}_{ext} \parallel c$-axis and $\boldsymbol{B}_{ext} \parallel b^*$-axis, respectively.

figure 4. At the lowest T about 30% of the total asymmetry is missing. This can be seen directly by comparing the early part of $P(t)$ at 3 K and at 300 K (see figure 5). Apparently part of the μSR signal is wiped out at low T, due to the presence of an extremely wide field distribution ($\gtrsim$1 kG) which leads to a very rapid loss of polarization by dephasing. The other unexpected observation is that the signal I which dominates at low temperatures decreases with rising temperature while signal II increases by the same proportion and eventually is the only remaining component at high T. What is really unusual about this is the fact that the disappearance of component I depends on the crystal orientation: for $\boldsymbol{B}_{ext} \parallel c$-axis, component I survives up to 150 K, while for the equivalent $\boldsymbol{B}_{ext} \parallel a$-axis or $\boldsymbol{B}_{ext} \parallel b^*$-axis, component I is already lost above 80 K. We will come back to these observations in section 6.

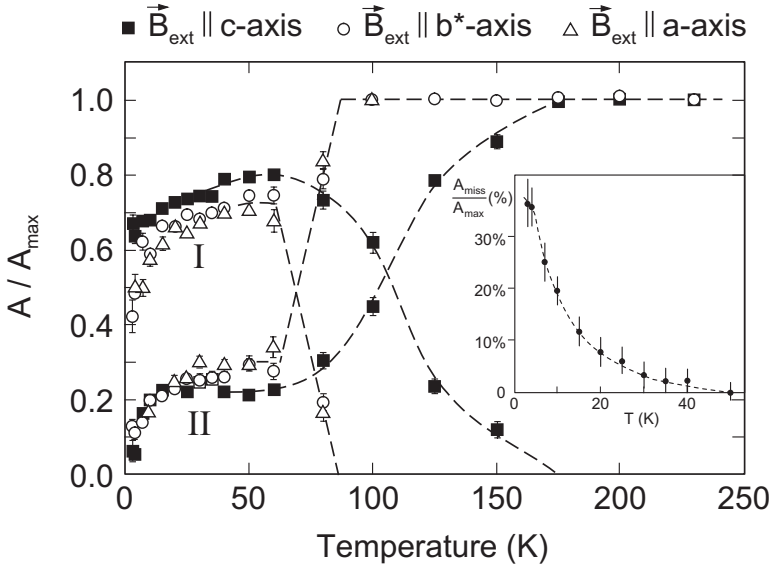

Figure 4. Temperature dependences of the amplitudes (asymmetries) A_1 (signal I) and A_2 (signal II) for $\boldsymbol{B}_{ext}$ oriented along one of the principal axes a, b^* and c. Note that there is no difference for the a, b^*-orientations (which are equivalent) but a significantly different behaviour is seen for $\boldsymbol{B}_{ext} \parallel c$-axis. The inset shows the temperature dependence of the missing asymmetry below 50 K. The data points displayed are averages over all three principal orientations. The dashed lines are guides to the eye.

The temperature dependences of the fitted relaxation rates λ_1 and λ_2 for $\boldsymbol{B}_{ext} \parallel c$-axis and $\boldsymbol{B}_{ext} \parallel b^*$-axis are reproduced in figure 6. The results for $\boldsymbol{B}_{ext} \parallel a$-axis are identical with the results for $\boldsymbol{B}_{ext} \parallel b^*$-axis and are not shown. They will be discussed further in section 6.

4. Determination of the μ^+ sites

The determination will follow from the analysis of the μ^+ Knight shift as discussed in detail in [8]. The Knight shift is calculated from the precession frequency as follows:

$$K = (\nu - \nu_0)/\nu_0 - \left(\frac{4\pi}{3} - N\right)\chi_v \tag{2}$$

where $(4\pi/3 - N)\chi_v$ is a correction accounting for the demagnetization field and the Lorentz field. N is the demagnetization factor and χ_v the magnetic susceptibility of the sample in units of emu cm^{-3}. ν_0 is the precession frequency corresponding to the external field

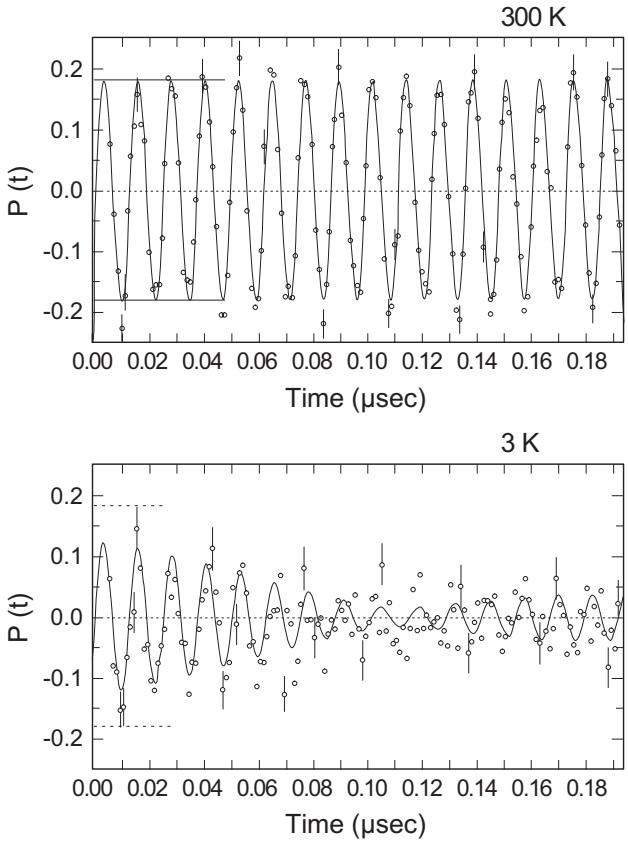

Figure 5. Time evolution of the μ^+ polarization, $P(t)$, as observed in the 'up' detector, in the first 190 ns at $T = 3$ K and 300 K. Note the reduction in amplitude at $T = 3$ K.

($\nu_0 = (\gamma_\mu/2\pi)B_{ext}$, $\gamma_\mu/2\pi = 13.553\,88$ kHz G^{-1}). B_{ext} has been measured by a NMR magnetometer with an accuracy of about 10 ppm. The demagnetization factor for the two crystals in their respective orientations has been estimated with the help of reference [12], resulting in $N(\text{No } 1) \simeq 0.44$ and $N(\text{No } 2) \simeq 0.38$, respectively. The susceptibility is taken from reference [2]. The thus-extracted Knight shifts as functions of temperature are displayed in figures 7(a), 7(b).

The Knight shift arises from a contact hyperfine-field contribution and a dipolar contribution from the field-induced moments on the Ce sites. For $\boldsymbol{B}_{ext}$ along the cartesian axes a, b^*, c we can write [8]

$$K_a = (A_c + A_{aa}^{dip})\chi_a \tag{3a}$$

$$K_{b^*} = (A_c + A_{b^*b^*}^{dip})\chi_{b^*} \tag{3b}$$

$$K_c = (A_c + A_{cc}^{dip})\chi_c \tag{3c}$$

where A_c is the isotropic contact coupling constant and A_{ii}^{dip} a diagonal element of the dipolar coupling tensor with

$$\mathrm{tr}(\overleftrightarrow{A}^{dip}) = 0 \tag{4}$$

and χ_i the appropriate susceptibility component (now in emu mol^{-1}!) Equations (3) imply that the K_i should scale with the χ_i. From the slopes of K_i versus χ_i and equation (4) all four

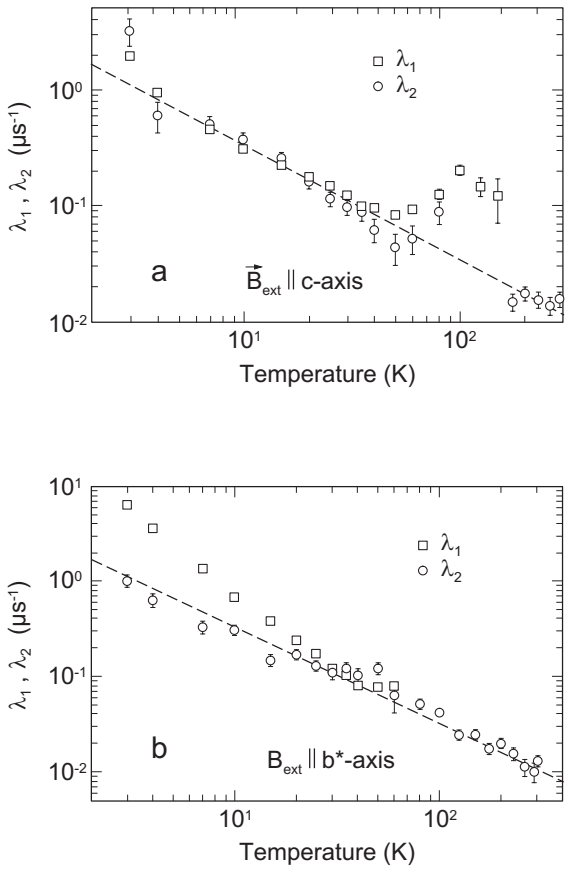

Figure 6. A log–log plot of the temperature dependence of the relaxation rates λ_1 and λ_2 for (a) $\boldsymbol{B}_{ext} \parallel c$-axis and (b) $\boldsymbol{B}_{ext} \parallel b^*$-axis. The dashed straight line denotes a $1/T$ dependence.

unknown coupling parameters can be readily obtained. However, in the present case we find that the K_i obtained do not scale with the bulk susceptibility χ_i over the full temperature range. Instead it is found that K_a, K_b^* and K_c for both components are excellently fitted in the range 3 K–60 K by a Curie–Weiss expression:

$$K_i = K_{0,i} + \frac{B_i}{T - T_{c,i}} \qquad (i = a, b^*, c) \tag{5}$$

implying that the relevant local susceptibility (i.e. the susceptibility of the μ^+ nearest-neighbour Ce ions) follows the same temperature dependence in contrast to the bulk susceptibility. The fitted parameters B_i, $K_{0,i}$ and $T_{c,i}$ are collected in table 1. The fits are shown in figures 7(a), 7(b); their quality is evident.

By comparison with equation (3) we write

$$B_i = A_i C = (A_c + A_{ii}^{dip})C \tag{6}$$

where $C = NJ(J+1)g_J^2\mu_B^2/3k_B$ is the Curie constant. Assuming that the effective moment, as in the bulk susceptibility, is given by the Hund's-rule value (2.54 μ_B) we get $C = 0.807$ and calculate from the fitted B_i the parameters A_i, collected also in table 1.

Comparing the fit results in table 1 for $\boldsymbol{B}_{ext} \parallel a$-axis and $\boldsymbol{B}_{ext} \parallel b^*$-axis we find them to be essentially equal, implying that $A_{aa}^{dip} = A_{b^*b^*}^{dip} = A_{\perp}^{dip}$ for both components, i.e. the dipolar

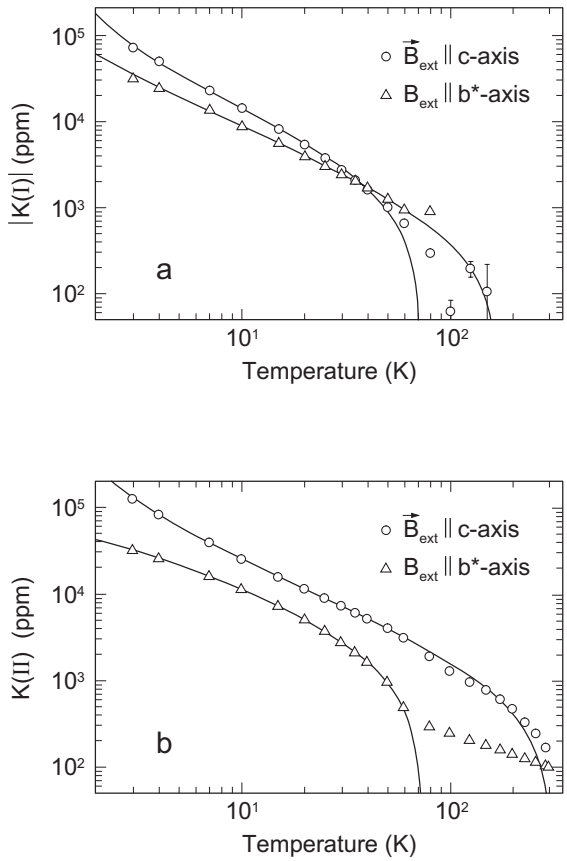

Figure 7. A log–log plot of the temperature dependence of the Knight shifts K_1 and K_2 (of signals I and II) for $\boldsymbol{B}_{ext} \parallel b^*$-axis and $\boldsymbol{B}_{ext} \parallel c$-axis, respectively. Note that K_1 is actually negative. The solid lines represent fits of equation (5) for $T \leqslant 60$ K. When not shown, the error bars on the data points are much smaller than the size of the symbols.

Table 1. Results from Curie–Weiss fits of the Knight shifts in the range 3 K–60 K ($C = 0.807$ emu mol^{-1}).

		$\boldsymbol{B} \parallel \boldsymbol{a}$	$\boldsymbol{B} \parallel \boldsymbol{b}^*$	$\boldsymbol{B} \parallel \boldsymbol{c}$
Signal I	$B = CA$	−0.086(1)	−0.087(1)	−0.140 (2)
	A (mol emu^{-1})	−0.106(2)	−0.108(2)	−0.174(3)
	K_0 (ppm)	525(26)	505(12)	1966(10)
	T_c (K)	1.08(6)	0.57(4)	1.208(5)
Signal II	$B = CA$	0.151(1)	0.152(1)	0.230 (1)
	A (mol emu^{-1})	0.187(2)	0.189(2)	0.285(2)
	K_0 (ppm)	−1827(25)	−2020(23)	−742(18)
	T_c (K)	−1.36(6)	−1.38(1)	1.24(1)
	$T_{c,bulk}$ (K)	−67	− 67	−24

coupling tensor is axially symmetric and (from equation (4))

$$A_{cc}^{dip} = A_{\parallel}^{dip} = -\frac{1}{2}A_{\perp}^{dip}. \tag{7}$$

This leads to the $\cos^2(\theta)$ dependence displayed in figure 3. Combining two of the equations (3), $A_{\parallel}^{dip}$ and A_c can be evaluated separately (see table 2).

Table 2. A_c and $A_{\parallel}^{dip}$ calculated from table 1.

	Signal I	Signal II
A_c (kG/μ_B)	−0.726(3)	1.240(3)
$A_{\parallel}^{dip}$ (kG/μ_B)	−0.246(2)	0.352(2)

On the other hand, above 100 K we find that the Knight shift K of the surviving component scales perfectly with the bulk susceptibility, as shown in figure 8. From the slopes we extract directly the coupling parameter A_i. No values for $\boldsymbol{B}_{ext} \parallel a$-axis are available for $T > 100$ K. Adopting the reasonable assumption that also in this temperature range $A_{aa}^{dip} = A_{b^*b^*}^{dip}$, we can again determine $A_{\parallel}^{dip}$ and A_c separately (see table 3).

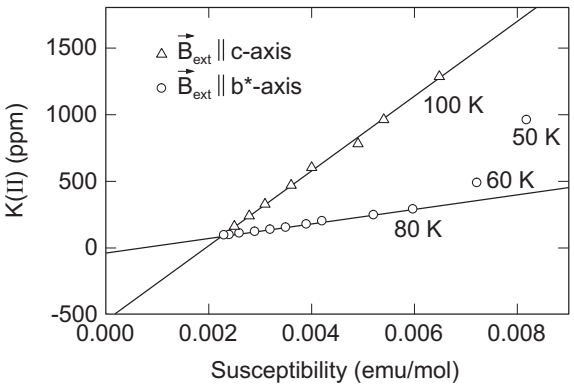

Figure 8. A Clogston–Jaccarino plot of K_2 versus χ_{bulk} for $T \geqslant 80$ K, showing the scaling of K_2 with χ_{bulk} for $\boldsymbol{B}_{ext} \parallel c$-axis and $\boldsymbol{B}_{ext} \parallel b^*$-axis in this temperature range.

Table 3. High-temperature coupling constants from K versus χ plots (only one signal).

	A (mol emu^{-1})	K_0 (ppm)	A_c (kG/μ_B)	$A_{\parallel}^{dip}$ (kG/μ_B)
$\boldsymbol{B} \parallel \boldsymbol{b}^*$	0.0554	−35	0.709	0.803
$\boldsymbol{B} \parallel \boldsymbol{c}$	0.271	−540	0.709	0.803

The fact that the dipolar coupling tensor is axially symmetric provides already a first clue to the possible sites. Consulting reference [13], only two types of interstitial site have the right point symmetry, namely (in Wyckoff notation) the a and b sites. The generic positions for the a site are $(00z)$ and $(00z + \frac{1}{2})$; only the positions with $z = 0$ and $z = 1/4$ provide a fully symmetric environment for the μ^+. For these positions one calculates $A_{\parallel}^{dip} = -2.2$ kG/μ_B and $A_{\parallel}^{dip} = +0.094$ kG/μ_B, respectively. Comparing these values with the values in table 2 and table 3 we conclude that the a site cannot be occupied.

Turning to the b site with the generic positions $(\frac{1}{3}\frac{2}{3}z)$ and $(\frac{2}{3}\frac{1}{3}z + \frac{1}{2})$ and considering figure 1, it appears very suggestive to place the μ^+ inside the tetrahedron made up of one Ce_1 ion and three Ce_3 ions. There are actually two such versions of tetrahedra which are

distinguished by their different enclosed volumes and by their next-nearest neighbours. In the first version these are three Ni ions (we call this the b_1 site) and in the second version three Ce_2 ions (the b_2 site), which is also the more spacious site (see figure 1). We can get from the b_1 site to the b_2 site by moving along the z-direction. Figure 9 shows $A_{\parallel}^{dip}$ calculated at $(\frac{1}{3}\frac{2}{3}z)$ as a function of z.

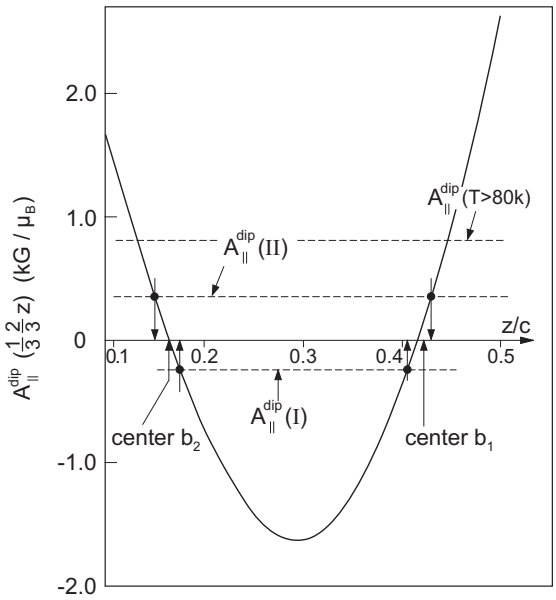

Figure 9. Calculated $A_{\parallel}^{dip}(z)$ along the line $(\frac{1}{3}\frac{2}{3}z)$ connecting the b_1 site and the b_2 site. The measured $A_{\parallel}^{dip}$ from signal I and signal II are indicated as horizontal lines. They cross with the calculated $A_{\parallel}^{dip}(z)$ at z-values near the centre of the b_1 and b_2 tetrahedra.

The geometrical centre of the b_1 position is at $z = 0.422$ and that of the b_2 position at $z = 0.162$. Also indicated by horizontal lines are the $A_{\parallel}^{dip}$ from tables 2 and 3. The two horizontal lines associated with components I and II for $T \leqslant 60$ K cross the calculated $A_{\parallel}^{dip}$ at z-values which are quite close to the geometrical centres of the b_1 and b_2 tetrahedra. In assigning one of the components to a particular position one could use the criterion of closest distance to the geometrical centre. On the basis of this (weak) criterion, signal I is assigned to μ^+ located at the b_2 site with $z \simeq 0.175$ and signal II to μ^+ located at the b_1 site with $z \simeq 0.43$. Alternatively, reversing the assignment, signal I would lead to $z \simeq 0.405$ and signal II to $z \simeq 0.15$.

Finally the high-temperature value of $A_{\parallel}^{dip} = 0.803$ kG/μ_B seems to indicate that the μ^+ has entered into a new state which we ascribe to rapid long-range μ^+ diffusion involving jumps between the b_1 and b_2 sites via the intervening interstitial c site (generic position $(\frac{1}{2}\frac{1}{2}\frac{1}{2})$, centre position in figure 1). One may speculate that this will shift the momentary μ^+ positions at the two b sites slightly closer to $z = \frac{1}{2}$, i.e. closer to the Ce_1 neighbours, with the effect that both $A_{\parallel}^{dip}$ will increase and so will their average (see figure 9).

In calculating $A_{\parallel}^{dip}$ we have assumed that the magnetic response is the same for all Ce^{3+} ions irrespective of their inequivalent lattice sites. This seems to be consistent with the perfect Curie–Weiss behaviour (with almost zero Curie–Weiss temperatures) of the Knight shifts for $T \leqslant 60$ K. If the response had been different, involving different Curie temperatures

T_c or some other different temperature dependence, no such behaviour could have been observed. The same can be said with respect to the observed scaling of K with the bulk susceptibility for $T > 100$ K.

5. Comparison of local and bulk susceptibility

In order to demonstrate the differences of the local and bulk susceptibilities we present in figure 10 log–log plots of the inverse susceptibilities versus $T - T_c$. According to equation (3) the local susceptibilities are given by

$$\chi_i(X) = \frac{K_i(X) - K_{0,i}(X)}{A_i(X)} = \frac{0.807}{T - T_{c,i}(X)}. \tag{8}$$

with $i = a, b^*, c$, $X = \mathrm{I}, \mathrm{II}$. Of course, all $\chi_i(X)^{-1}$ fall on the same line with a slope of 1/0.807. In contrast the bulk susceptibilities for $\boldsymbol{B}_{ext} \parallel c$-axis and $\boldsymbol{B}_{ext} \parallel b^*$-axis merge with this line only above 100 K and show a drastically different behaviour below, reflecting the deviation from the Curie–Weiss behaviour. This deviation is ascribed to crystal-field effects. Unfortunately the CEF splitting of the Ce^{3+} $^2F_{5/2}$ ground-state multiplet is not known. By analogy with other hexagonal Ce compounds it is thought that the ground state and the two first excited states are all doublets. From high-temperature specific heat measurements the CEF splitting between the ground-state doublet and the first excited doublet is estimated to be 240 K [13]. This is consistent with a preliminary inelastic neutron scattering measurement which places a lower limit of about 10 meV on the gap between the ground state and the first excited doublet [14]. The very different behaviour of the local susceptibility for $T \leqslant 60$ K, regarding not only the temperature dependence but also the nearly isotropic behaviour, must be muon induced. It is to be expected that the presence of the μ^+ will modify the electric field at the four nearest (three Ce_3, one Ce_1) and, for the b_2 site, also the three next-nearest (three Ce_2) neighbours and, consequently, may alter the magnetic response of these ions, as has been observed in other rare-earth- and U-based intermetallic compounds which, however, all possess singlet ground states [15–17]. In the present case it appears that one observes a quasi-free Ce^{3+} ionic state, implying a much reduced CEF splitting. This aspect will be studied in future work.

6. Discussion of signal amplitudes (asymmetries) and relaxation rates

We have already mentioned that at low T about 30% of the implanted μ^+ become invisible (see the inset in figure 4). The missing asymmetry implies that a corresponding fraction of μ^+ are depolarized so quickly, within the dead time of the spectrometer, that their signal appears to be wiped out. This requires that the relaxation time T_2 is less than $\sim$10 ns which in turn implies that those muons are exposed to a very wide field distribution of $\Delta B \gtrsim 1/(\gamma_\mu T_2) \simeq 1$ kG. Such a wide field distribution is difficult to get in the paramagnetic state (remember that $B_{ext} = 0.6$ T). It would imply that we have a spread in Knight shifts of $\gtrsim$16%. Actually below 4 K, we find Knight shifts of this order, but it seems impossible to find a spread of similar magnitude in a single crystal. Also, although the fraction of the sample associated with the missing asymmetry decreases with rising temperature and vanishes around 50 K, the field spread ΔB appears to remain above 1 kG. Alternatively the large field spread may be associated with a magnetically ordered phase, persisting above T_N in part of the sample. ZF μSR measurements below T_N do indeed show a loss of asymmetry [7]. The ordering temperature involved must be even higher than 50 K since ΔB inside the ordered volume fraction does not seem to shrink. Whatever the true explanation may be, we are faced

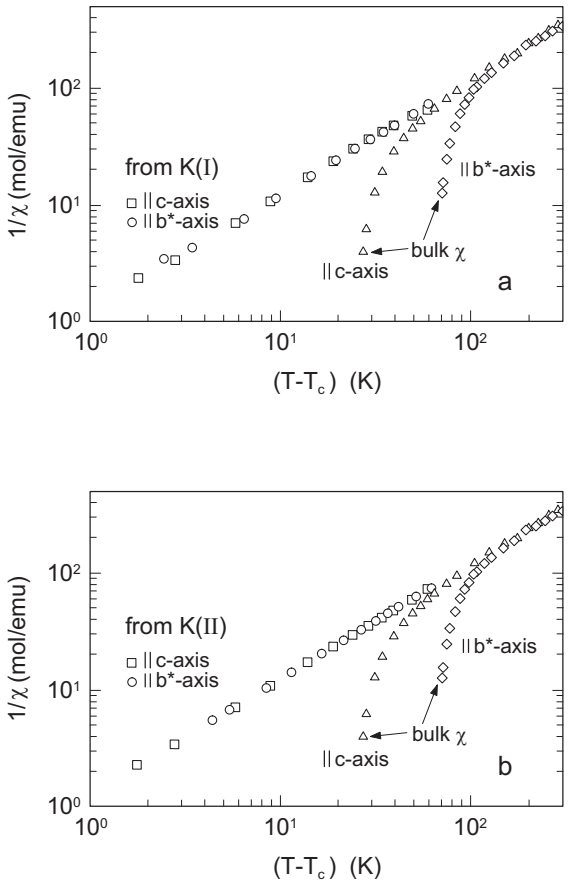

Figure 10. Log–log plots of the inverse bulk susceptibilities, χ_b, and the inverse local susceptibilities extracted from the $K_i(T)$ for $T \leqslant 60$ K (equation (6)), versus $T - T_{c,i}$. The various $T_{c,i}$ are taken from table 1; (a) from signal I, (b) from signal II. Note the lack of anisotropy in the local susceptibilities in contrast to χ_{bulk} and the coincidence of all data above 100 K. χ_{bulk} is taken from reference [2].

with the question of whether the observed phenomenon is an intrinsic property (that would also be observed in the most perfect crystal) or is related to the sample quality. We can exclude foreign phases because their presence should not depend on temperature. At this point we cannot offer any convincing explanation for the loss of asymmetry.

As pointed out in section 3 the signal amplitudes also show a peculiar behaviour at higher temperatures in that the relative change of the two amplitudes depends on the orientation of the sample with respect to the applied field $\boldsymbol{B}_{ext}$ (see figure 4). From the fact that the same behaviour is seen for $\boldsymbol{B}_{ext} \parallel a$-axis and $\boldsymbol{B}_{ext} \parallel b^*$-axis, involving two different crystals and different parts of the cylinder surfaces, we conclude that it is really the orientation of the applied field with respect to the crystal axes which matters. Since the two Knight shifts deviate above 60 K from the Curie–Weiss behaviour discussed above and are also not scaling with the bulk susceptibility (see figures 7, 8) it is clear that we are not observing a relative change of population of the two b sites, assuming a stationary μ^+, but also that there is no long-range diffusion as in the temperature range where only one signal is observed. Rather, it seems that we are monitoring the onset of diffusion which initially may just consist in a forth-and-back

jumping between nearest-neighbour b_1 and b_2 sites along the c-axis direction (see figure 1) before long-range diffusion via the c site is energetically possible. The fact that the extent of this transient phase depends on the orientation of $\boldsymbol{B}_{ext}$ in the crystal frame suggests that magnetostriction may play an important role in adjusting the effective potential depth of the two b sites. Future studies of this as a function of applied field strength will we hope allow us to test this conjecture.

Finally we briefly discuss the observed relaxation rates displayed in figure 6. Compared with low-TF (40 G) measurements [7] the present values at 0.6 T are enhanced by roughly a factor of 5, much less than the ratio 6 kG/0.04 kG = 150. This implies that the observed relaxation rates are only in part induced by B_{ext}, i.e. by inhomogeneous line broadening, but that there is a substantial relaxation of probably dynamical origin. This may explain the observation that the relaxation is best fitted with an exponential function. Figure 6(a) ($\boldsymbol{B}_{ext} \parallel c$-axis) reveals that below 60 K, λ_1 and λ_2 follow a $1/T$ behaviour. Above that temperature we find a significant increase in both λ_1 and λ_2, followed by a drastic decline above 150 K. We ascribe this increase to the onset of diffusion as discussed above and in section 4. This will lead initially to a line broadening and with increasing jump rate to a collapse of the splitting and the emergence of a single line [17, 18]. Figure 6(b) ($\boldsymbol{B}_{ext} \parallel b^*$-axis) displays a different picture. λ_1 and λ_2 become quite different below 30 K and only λ_2 seems to follow an overall $1/T$ dependence. No enhancement of λ_1 and λ_2 around 100 K is seen. This is consistent with the much smaller Knight shifts and therefore reduced fluctuating field amplitudes when the μ^+ hop between the b_1 and b_2 sites.

7. Conclusions and summary

The present investigation has revealed a number of puzzling properties concerning not only the behaviour and influence of the implanted μ^+, but also of the Ce_7Ni_3 system itself. The latter implies that we do not yet have full knowledge and understanding of this system (or at least of the individual samples investigated) in its paramagnetic phase and that more work is certainly needed concerning the metallurgy of this system and such properties as magnetostriction, temperature dependence of lattice parameters, elastic properties and CEF effects. Below we summarize our findings.

Transverse-field (TF) μSR measurements in an applied field of 0.6 T revealed two components (I, II) of which the muon Knight shifts, relaxation rates and amplitudes (asymmetries) have been determined as functions of temperature and for the three principal orientations $\boldsymbol{B}_{ext} \parallel a$-axis, $\boldsymbol{B}_{ext} \parallel b^*$-axis and $\boldsymbol{B}_{ext} \parallel c$-axis. A missing asymmetry below 50 K, growing to more than 30% of the full amplitude at 3 K, signalled a third fraction of muons which reflect either the presence of a magnetically ordered phase above $T_N = 1.9$ K or some huge spread of Knight shifts in a fraction of the sample volume. We have no explanation yet for this signal.

Another puzzling observation is that one of the two components (labelled I) became depopulated at higher temperatures, but this depended on the orientation of the single crystals: for $\boldsymbol{B}_{ext} \parallel c$-axis, component I disappeared for $T > 150$ K; however, for $\boldsymbol{B}_{ext} \parallel a$-axis or $\boldsymbol{B}_{ext} \parallel b^*$-axis, it disappeared above 80 K. We suggest that this behaviour may be caused by magnetostriction affecting the onset and type of μ^+ diffusion.

Below 60 K the Knight shift, for both components and for all orientations, follows perfectly a Curie–Weiss behaviour with Curie temperatures around ± 1 K in striking contrast to the bulk susceptibility behaviour. However, above 100 K the Knight shift of the remaining or dominant signal scales with the bulk susceptibility. From the Knight shifts we extracted the dipolar

coupling tensor which then allowed us to assign the μ^+ to particular lattice sites: these sites are b sites (in Wyckoff notation) with generic positions of $(\frac{1}{2}\,\frac{2}{3}0.175)$ and $(\frac{1}{2}\,\frac{2}{3}0.43)$ for signal I and signal II, respectively. Alternatively, reversing the site assignment, signal I is associated with the position $(\frac{1}{2}\,\frac{2}{3}0.405)$ and signal II with the position $(\frac{1}{2}\,\frac{2}{3}0.15)$. Above 100 K a different state is found in which the μ^+ seems to hop quickly on the network of b_1 and b_2 sites linked via the c sites. This seems to be consistent with an enhanced relaxation rate in the temperature range 60–100 K where the onset of μ^+ diffusion should initially lead to a line broadening followed by a collapse of the splitting. The Curie–Weiss behaviour of the muon Knight shift below 60 K translates into an isotropic Curie–Weiss susceptibility of the nearest and perhaps next-nearest Ce neighbours, implying that these Ce^{3+} ions behave essentially like free Ce^{3+} ions. We suggest that this is a muon-induced effect which reduces the CEF splitting of the $^2F_{5/2}$ ground-state multiplet of the nearest and perhaps next-nearest Ce neighbours drastically.

It should also be pointed out that the temperature-independent Knight-shift constants $K_{0,i}(X)$ (see tables 2 and 3) are very anisotropic rather than showing an isotropic behaviour as is normally expected. This observation seems to indicate that the $K_{0,i}(X)$ are not arising from just the Pauli paramagnetism of the conduction electrons, but that somehow the f electron states are also involved.

Acknowledgments

We thank the PSI accelerator crew and the PSI μSR facility group, in particular Dr A Amato, for providing excellent measuring conditions. This work was in part supported by the Swiss National Science foundation, a Grant-in-Aid for Scientific Research from the Ministry of Education, Science and Culture of Japan and by the BMBF (Germany) under contract 03-KA4-TUI-9.

References

[1] von Löhneysen H 1996 *J. Phys.: Condens. Matter* **8** 9689
[2] Umeo K, Kadomatsu H and Takabatake T 1996 *J. Phys.: Condens. Matter* **8** 9743
[3] Roof R B, Larson A C and Cromer D T 1991 *Acta Crystallogr.* **14** 1084
[4] Sereni J G, Trovarelli O, Kappler J P, Poschke C, Trappmann T and von Löhneysen H 1994 *Physica* B **199+200** 567
[5] Kadowaki H, Motoya V, Kawasaki T, Osakabe T, Okumura H, Kakurai K, Umeo K and Takabatake T 2000 *J. Phys. Soc. Japan* **69** 2269
[6] Umeo K, Takabatake T, Sato N, Komatsubara T, Oda K and Kindo K 1997 *J. Phys. Soc. Japan* **66** 2133
[7] Kalvius G M *et al* to be published
[8] See e.g. Schenck A 1999 *Muon Science (Scottish Universities Summer School in Physics 51) (St Andrews, 1998)* ed S L Lee, R Cywinski and S H Kilcoyne (Bristol: Institute of Physics Publishing)
[9] Schenck A, Pinkpank M, Gygax F N, Neumann K-U, Ziebeck K R A and Amato A 1998 *J. Phys.: Condens. Matter* **10** 8054
[10] Umeo K, Takabatake T, Ohmoto H, Pietras T, von Löhneysen H, Koyama K, Hane S and Goto T 1998 *Phys. Rev.* B **58** 12 095
[11] Umeo K *et al* 2001 private communication
[12] Akishin P G and Gaganov I A 1992 *J. Magn. Magn. Mater.* **110** 175
[13] *International Tables for Crystallography* 1987 vol A, ed T Hahn (Dordrecht: Reidel)
[14] Clementyev E *et al* 2000 preliminary data obtained at PSI
[15] Feyerherm R, Amato A, Grayevski A, Gygax F N, Kaplan N and Schenck A 1995 *Z. Phys.* B **99** 3
[16] Tashma T, Amato A, Grayevski A, Gygax F N, Pinkpank M, Schenck A and Kaplan N 1997 *Phys. Rev.* **56** 9397
[17] See e.g. Abragam A 1970 *The Principles of Nuclear Magnetism* (Oxford: Oxford University Press) p 447 ff
[18] Alexandrowicz G, Tashma T, Socolovsky M, Amato A, Grayevski A, Gygax F N, Pinkpank M, Schenck A and Kaplan N 1999 *Phys. Rev. Lett.* **82** 1028